Reorganization Asymmetry of Electron Transfer in Ferroelectric Media and Principles of Artificial Photosynthesis

Dmitry V. Matyushov*

Department of Chemistry and Biochemistry and the Center for the Early Events in Photosynthesis, Arizona State University, PO Box 871604, Tempe, Arizona 85287-1604

Received: February 27, 2006

This study considers electronic transitions within donor−acceptor complexes dissolved in media with macroscopic polarization. The change of the polarizability of the donor−acceptor complex in the course of electronic transition couples to the reaction field of the polar environment and the electric field created by the macroscopic polarization. An analytical theory developed to describe this situation predicts a significant asymmetry of the reorganization energy between charge separation and charge recombination transitions. This result is proved by Monte Carlo simulations of a model polarizable diatomic dissolved in a ferroelectric fluid of soft dipolar spheres. The ratio of the reorganization energies for the forward and backward reactions up to a factor of 25 is obtained in the simulations. This result, as well as the effect of the macroscopic electric field, is discussed in application to the design of efficient photosynthetic devices.

I. Introduction

Electron transfer (ET) reaction is a basic elementary step in photoinduced charge separation occurring in both natural and artificial photosynthesis. The fundamental mechanism behind the conversion of light energy into the energy of a charge-separated state is illustrated in Figure 1. Optical excitation $h\nu$ of the donor unit, D → D*, within the donor−acceptor complex, D−A, lifts the energy level of the donor to create conditions for the photoinduced charge separation step, D*−A → D^+−A^-. Charge separation is generally an activated transition. The activation barrier, according to the Marcus−Hush theory,[1] can be obtained from the equilibrium free energy gap between the final and initial ET states, ΔF_0, and the free energy λ required to reorganize the nuclear degrees of freedom (reorganization free energy). When the equilibrium free energy of the acceptor is below the free energy of the donor by the amount of free energy λ, the charge separation transition is activationless. Such an activationless transition is often fast and efficient, but it requires losing the energy λ from the photon energy $h\nu$. Increasing the energetic efficiency of photosynthesis therefore demands λ to be as low as possible. It is often assumed that an important role played by the hydrophobic protein matrix in facilitating ET in natural photosynthesis is to screen highly polar aqueous environment and to reduce λ.

Once the charge-separated state has been created, it needs to be sufficiently long-lived to be used for energy storage. A mechanism often suggested to be of primary importance in natural systems is the use of a sequence of activationless ET steps to move the electron away from the primary donor. Each activationless step i lowers the system energy by λ_i thus resulting in the overall low energetic efficiency of the photosynthetic unit. The reaction competing with photoinduced charge separation is the normally highly exothermic return electron transfer to the ground D−A state. The classical reaction path then goes through the relatively high activation barrier in the inverted ET region predicted by the Marcus−Hush theory (point "C" in Figure 1).[1] However, the system avoids this activated path by nearly activationless transfer to a vibrationally excited state, D−A(v), of the electronically ground donor−acceptor complex (dashed line in Figure 1). The vibrational energy is subsequently released to heat through vibrational relaxation (v → 0 in Figure 1).

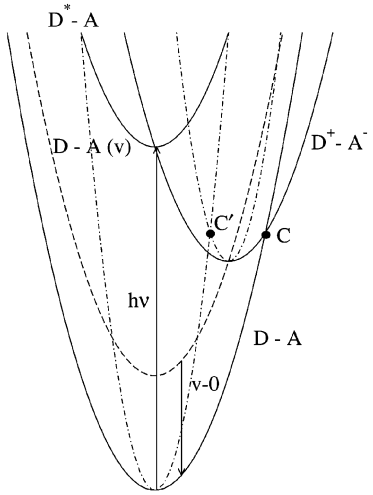

Figure 1. Energetics of photoinduced electron-transfer involved in natural and artificial photosynthesis. The charge-separated state D^+−A^- is placed below the photoexcited-state D*−A by the reorganization energy λ to ensure activationless transition. The dash−dotted line marks the free energy surface of the initial state D−A with the reorganization energy four times lower than the value of λ used to draw the free energy surfaces shown by the solid lines. The dashed line indicates the vibrationally excited electronic ground state for which the recombination transition D^+−A^- → D−A does not require an activation barrier. C and C′ indicate the classical transition states.

The design of an optimization of a sequence of activationless ET reactions requires a very precise molecular tuning, which is hard to achieve in synthetic systems despite some significant progress achieved in this field in recent years.[2,3] It is therefore desirable to search for mechanisms of reducing the rate of return

* E-mail: dmitrym@asu.edu.

10.1021/jp061240p CCC: $33.50
Published on Web 05/03/2006

ET in molecular photosynthesis with the goal of achieving higher quantum yield for the charge-separated state. According to the current understanding of radiationless transitions in molecules,[4] an efficient way to reduce the return rate would be to move the reaction into the normal region of ET.

The electronic states D*−A and D−A are distinct, and, in principle, the charge-recombination transition $D^+-A^- \rightarrow D-A$ can be characterized by a pair of parabolas with the curvatures different from those of the charge-separation transition $D^*-A \rightarrow D^+-A^-$. In the reactions classification adopted here we label transition $D^*-A \rightarrow D^+-A^-$ as charge separation and transition $D^+-A^- \rightarrow D-A$ as charge recombination. Backward transitions at each step are not considered as separate steps in the reaction mechanism. When the photoexcitation energy is kept constant, shifting the recombination reaction into the normal region would require increasing the curvature of the charge-recombination parabolas (dash−dotted lines in Figure 1), i.e., lowering the reorganization energy. The inverted-region activated state C then shifts to the normal-region activated state C′ in Figure 1.

It is easy to realize the pitfall of the picture shown in Figure 1. The separation of the minima of two dash−dotted parabolas must be equal, in the Marcus−Hush theory, to twice the reorganization energy, which is clearly violated once the curvature is increased without corresponding shift of the parabolas. Therefore, the goal of bringing the recombination reaction to the normal region can be realized only within models extending beyond the Marcus−Hush picture of equal-curvature parabolas. One needs flexibility, built into the model, that would allow decoupling of the Stokes shift from the curvatures. The use of parabolic free energy surfaces with different curvatures, as was suggested by Kakitani and Mataga,[5] is prohibited by the requirement of energy conservation. When the energy gap between the donor and acceptor energy levels is taken for the reaction coordinate, the free energy surfaces of the initial, $F_1(X)$, and final, $F_2(X)$, ET states are connected by the linear relation established by Warshel[6] and Tachiya[12]

$$F_2(X) = F_1(X) + X \tag{1}$$

The parabolic surfaces with different curvatures clearly violate this requirement and, therefore, cannot be used for the modeling of ET reactions. The problem can be resolved within a three-parameter model of ET free energy surfaces[13] which allows different reorganization energies and, at the same time, does not violate eq 1. The free energy surfaces $F_i(X)$ are then necessarily nonparabolic.

Once different reorganization energies are allowed within a theory of free energy surfaces, one needs to address the following major question: What would be a mechanism resulting in dramatic changes of reorganization energies between charge separation and charge recombination reactions? A question relevant to studies of natural photosynthesis is the following: Is the role of the protein matrix reduced to providing a low dielectric constant or are there some other properties of proteins beneficial for high efficiency of natural photosynthesis? Note that shifting the transition point from C to C′ requires a very significant change in the reorganization energy (a factor of 4 decrease in Figure 1). The possibility of different equilibrium-point curvatures of the two ET free energy surfaces has been actively pursued in the past decades by computer simulations searching for the effects of nonlinear solvation on ET.[6−11] However, in essentially all reports, the difference in reorganization energies between the initial and final ET states has never come close to the magnitude that would dramatically change the mechanism of charge recombination.

In this paper, we address the problem of reorganization asymmetry by considering ET reactions in polarizable donor−acceptor complexes immersed in polarization anisotropic media. A part of the motivation for this approach comes from studies of bacterial photosynthesis. The protein matrix in natural bacterial reaction centers is highly anisotropic with the electric field amounting to $\simeq 10^7$ V/cm.[14] On the other hand, the primary pair is highly polarizable with the polarizability change upon photoexcitation about 800−1100 Å^3.[15] Since bacteriochlorophyll cofactors are much less polarizable,[16] primary charge separation occurs with a large negative polarizability change. On a more fundamental level, polarizability change in the course of ET leads to very significant reorganization asymmetry, as follows from both analytical theories[17] and computer experiment.[18,19] The asymmetry arising from the coupling of changing polarizability to the solvent recation field is by far the largest achieved so far in computer simulations thus promising the desired alteration of the energetics of photosynthetic reactions.

In section II, we present an analytical model of ET free energy surfaces when both the polarizability and the dipole moment of the donor−acceptor complex change in the course of ET. The donor−acceptor complex is immersed in a polar medium which, in addition to usual polar response, is characterized by a macroscopic electric field. To mimic high electric fields present in molecular systems (thin films, proteins, etc.), we use a polar model fluid capable of producing ferroelectric order (section III). The ordered phase is obtained by Monte Carlo (MC) simulations. The possibility of ferroelectric order in bulk polar fluids is still actively debated in the literature,[20−22] and it has been suggested that boundary conditions employed in the simulation protocol significantly affect the possibility of creation of the macroscopically polar phase.[23] For our current purpose, this subject is not relevant since we are mostly interested in reactions in condensed phases with macroscopic electric fields strong enough to influence properties of electronic transitions. Whether the macroscopic polar order is stabilized by surface effects or some other reasons is not central to our study. On the other hand, ferroelectrics and ordered polar films may be used as solvents for ET reactions. The present analysis then directly applies to such systems. We return to discussing the role of reorganization asymmetry in improving the efficiency of photosynthesis in section IV.

II. Energetics of Electron Transfer

A. Model. Consider a donor−acceptor complex immersed in a medium with a nonzero macroscopic electric field **F**. The complex has the dipole moments $\mathbf{m}_{0i}$ and polarizabilities α_{0i} in two electronic states, $i = 1, 2$. These states are coupled to nuclear fluctuations in the solvent and are "dressed" with the field of the electronic solvent polarization following adiabatically the changes in the charge distribution within the complex. Because of the electronic polarization, the dipole moments and polarizabilities are different from their gas-phase values $\mathbf{m}_{0i}$ and α_{0i}[17]

$$\mathbf{m}_i = [\mathbf{1} - 2\alpha_{0i}\cdot\mathbf{a}_e]^{-1}\cdot\mathbf{m}_{0i} \tag{2}$$

and

$$\alpha_i = [\mathbf{1} - 2\alpha_{0i}\cdot\mathbf{a}_e]^{-1}\cdot\alpha_{0i} \tag{3}$$

Here, $\mathbf{a}_e$ is the linear response function such that the free energy of solvation of dipole $\mathbf{m}_0$ by the electronic solvent polarization (subscript "e") is $\mathbf{m}_0\cdot\mathbf{a}_e\cdot\mathbf{m}_0$. Once the electronic degrees of freedom have been adiabatically eliminated, the electronic

energy levels of the charge-transfer complex are affected by the microscopic nuclear field $\mathbf{R}_n$ (nuclear reaction field, subscript "n") and the macroscopic field $\mathbf{F}$ of the solvent[17]

$$E_i[\mathbf{R}_n] = I_i^{np} - \mathbf{m}_i\cdot(\mathbf{R}_n + \mathbf{F}) - \frac{1}{2}(\mathbf{R}_n + \mathbf{F})\cdot\alpha_{0i}\cdot(\mathbf{R}_n + \mathbf{F}) \quad (4)$$

Here I_i^{np} values are the energies of the ET complex which include the gas-phase energies and free energies of solvation by the solvent electronic polarization expressed as a sum of induction and dispersion solvation components.

The system Hamiltonian

$$H_i[\mathbf{R}_n] = E_i[\mathbf{R}_n] + H_B[\mathbf{R}_n] \quad (5)$$

is the sum of energies $E_i[\mathbf{R}_n]$ and the solvent bath Hamiltonian H_B. The Gaussian (linear response) approximation is adopted for the latter

$$H_B[\mathbf{R}_n] = \frac{1}{4}\mathbf{R}_n\cdot\mathbf{a}_n^{-1}\cdot\mathbf{R}_n \quad (6)$$

where $\mathbf{a}_n$ is the linear response function of the solvent nuclear polarization. In the following, for simplicity, we will assume collinear dipole moments $\mathbf{m}_i$ and the polarizability changing its value only along the direction of the dipole moment. We will also assume that the solute polarizability increases for the $1 \rightarrow 2$ transition, i.e., $\Delta\alpha = \alpha_2 - \alpha_1 > 0$. These approximations allow us to consider $\mathbf{a}_n$ as a scalar with the only nonzero projection along the solute dipole. We will also define the scalar F_m as the projection of the external field $\mathbf{F}$ on the direction of the solute dipole moment. The consideration of a more general case does not present fundamental difficulties.[17]

B. Free Energy Surfaces. The classical Hamiltonian $H_i[\mathbf{R}_n]$ in eq 5 can be used to build the free energy surfaces of ET along the reaction coordinate associated with the fluctuating donor−acceptor energy gap

$$X = \Delta H[\mathbf{R}_n] = H_2[\mathbf{R}_n] - H_1[\mathbf{R}_n] \quad (7)$$

The free energy surfaces for the initial ($i = 1$) and final ($i = 2$) ET states are obtained by constrained integration over the nuclear reaction field

$$e^{-\beta F_i(X)} = A\int \delta(X - \Delta H[\mathbf{R}_n])\, e^{-\beta H_i[\mathbf{R}_n]}\, d\mathbf{R}_n \quad (8)$$

where A is used to account for the units of the field $\mathbf{R}_n$ and $\beta = 1/k_BT$.

The Gaussian integral in eq 8 can be taken exactly with the result

$$F_i(X) = -\kappa_i X - \beta^{-1}\ln\left[\frac{\sinh\chi(X)}{\chi(X)}\right] \quad (9)$$

where

$$\chi(X) = 2\beta\sqrt{\kappa_i^3\lambda_i(X_0 - X)} \quad (10)$$

The parameters in eqs 9 and 10 are related to the properties of the polarizable donor−acceptor complex and the polar solvent by the following set of equations. The parameters κ_i are

$$\kappa_i = (2a_n f_{ni}\Delta\alpha)^{-1} \quad (11)$$

The parameter f_{ni} in eq 11 is responsible for the enhancement of the effective solute dipole by the interaction of the solute polarizability with the nuclear reaction field (cf. eqs 2 and 3)

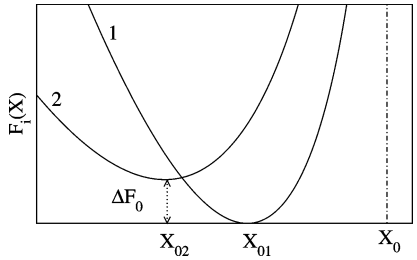

Figure 2. Free energy surfaces of ET $F_i(X)$ for the initial ($i = 1$, "1") and final ($i = 2$, "2") ET states. Shown in the plot are the free energy minima X_{0i}, the free energy gap $\Delta F_0 = F_{02} - F_{01}$, and the upper boundary X_0 for the reaction coordinate X.

$$f_{ni} = (1 - 2a_n\alpha_i)^{-1} \quad (12)$$

Further

$$X_0 = I_2^{np} - I_1^{np} - \Delta m F_m - \frac{1}{2}\Delta\alpha F_m^{\,2} + \frac{(\Delta m + \Delta\alpha F_m)^2}{2\Delta\alpha} \quad (13)$$

is the boundary of the fluctuation band of the reaction coordinate X (Figure 2). The requirement $X < X_0$, implicit in the definition of $\chi(X)$ is eq 10, does not allow the energy gap fluctuations to exceed X_0. Finally, λ_i in eq 10 is the solvent reorganization energy

$$\lambda_i = a_n f_{ni}[\Delta m + \Delta\alpha(R_i + F)]^2 \quad (14)$$

where $\Delta m = m_2 - m_1$ and reaction field R_i is

$$R_i = 2a_n f_{ni} m_i \quad (15)$$

The function $\chi(X)$ in eq 9 does not carry an index specifying the ET state because of the relation connecting the parameters of the two ET states

$$\kappa_1^{\,3}\lambda_1 = \kappa_2^{\,3}\lambda_2 \quad (16)$$

In addition, the parameters κ_1 and κ_2 are related by the additivity constant

$$\kappa_1 - \kappa_2 = 1 \quad (17)$$

The free energy surfaces defined in the range $X < X_0$ are nonparabolic, as is depicted in Figures 2 and 3. Each of them passes through the minimum at $X = X_{0i}$ defined by the condition

$$dF_i(X)/dX|_{X=X_{0i}} = 0 \quad (18)$$

This equation can be reduced to the algebraic equation for $\chi(X)$ which always has a nonzero solution

$$\chi\coth\chi - 1 = (2\beta\kappa_i^{\,2}\lambda_i)^{-1}\chi^2 \quad (19)$$

The solution is simplified when $\chi_{0i} = \chi(X_{0i}) \gg 1$. One then gets

$$X_{0i} = X_0 - \kappa_i\lambda_i \quad (20)$$

and the free energy at the minimum is

$$F_{0i} = -\kappa_i X_0 - \kappa_i^{\,2}\lambda_i \quad (21)$$

In this limit, the second derivatives taken at the position of the

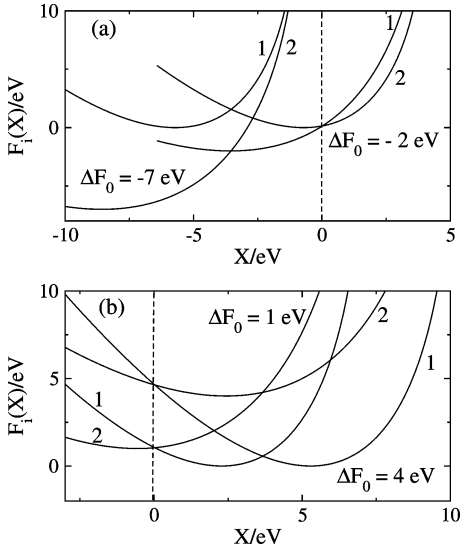

Figure 3. Free energy surfaces $F_i(X)$ at $\lambda_1 = 1$ eV and $\lambda_2 = 2$ eV. The free energy gap ΔF_0 is -2 eV and -7 eV in (a) and 1 and 4 eV in (b). The free energy surfaces corresponding to $\Delta F_0 = -7$ eV in (a) do not have the classical crossing point $X = 0$ indicated by the dashed lines in both panels.

minima define the two solvent reorganization energies, as is the case in standard formulations of ET theories

$$\left.\frac{d^2F_i(X)}{dX^2}\right|_{X=X_{0i}} = \frac{1}{2\lambda_i} \tag{22}$$

Note that from eq 21 the fluctuation boundary X_0 is related to the free energy gap $\Delta F_0 = F_{02} - F_{01}$ and two reorganization energies by the relation

$$X_0 = \Delta F_0 + \kappa_2{}^2\lambda_2 - \kappa_1{}^2\lambda_1 \tag{23}$$

Taken together, eqs 9−23 provide an exact model for the free energy surfaces of ET (Figure 2) based on three thermodynamic parameters, λ_1, λ_2, and ΔF_0. The present model thus extends the two-parameter Marcus−Hush theory, based on the assumption $\lambda_1 = \lambda_2$,[1] to three-parameter space. In view of the connection between κ_1 and κ_2 (eq 17), one of them can be considered as the nonparabolicity parameter

$$\kappa = \kappa_1 = \left(1 - \sqrt[3]{\frac{\lambda_1}{\lambda_2}}\right)^{-1} \tag{24}$$

In terms of the solute polarizability and the solvent nuclear response function, the nonparabolicity parameter becomes

$$\kappa = \frac{1 - 2a_n\alpha_1}{2a_n\Delta\alpha} \tag{25}$$

Because of the choice $\Delta\alpha > 0$ adopted here, $\lambda_1 < \lambda_2$ and $\kappa_i > 0$.

It is easy to prove that $F_i(X)$ from eq 9 obeys the energy conservation requirement given by eq 1. Note that the present model exhausts the space of thermodynamic parameters available for the description of ET reactions. Only three thermodynamic parameters, free energy gap between the minima and second cumulants of the fluctuations around the minima, are allowed by the two-state nature of the problem. Any extension of the theory for ET free energy surfaces beyond the present level will require nonequilibrium parameters to be involved.

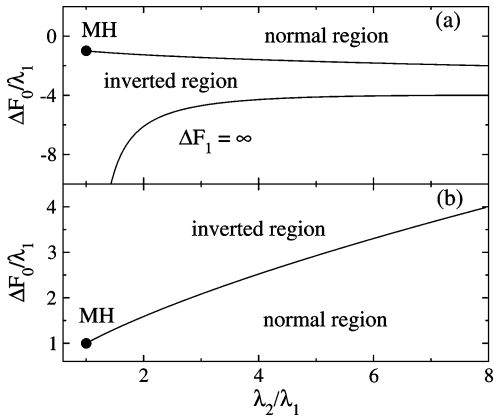

Figure 4. Normal and inverted region in the space of parameters $\Delta F_0/\lambda_1$ and λ_2/λ_1. Shown are the results for the forward reaction $1 \rightarrow 2$ (a) and for the backward reaction $2 \rightarrow 1$ (b). The quantum tunneling region with $\Delta F_1 = \infty$ in (a) is separated from the inverted region by the condition $X_0 = 0$, which puts the classical crossing point outside the range of reaction coordinates $X < X_0$ allowed by the condition of thermodynamic stability. The dots labeled as "MH" refer to the Marcus−Hush limit in which the transition from the normal to inverted region is given by the conditions: $\Delta F_0/\lambda = -1$ for $1 \rightarrow 2$ and $\Delta F_0/\lambda = 1$ for $2 \rightarrow 1$.

The requirement of thermodynamic stability of the polarization fluctuations limits the range of possible values of the reaction coordinate, $X \le X_0$. The reaction coordinate boundary X_0 is shown by the dash−dotted line in Figure 2. There is no singularity of $F_i(X)$ at $X = X_0$ and the free energies $F_i(X)$ are infinite at $X > X_0$. For reaction coordinates sufficiently far from X_0, the free energy surfaces can be conveniently rewritten in the form

$$F_i(X) = F_{0i} + \kappa_i[\sqrt{X_{0i} + \kappa_i\lambda_i - X} - \sqrt{\kappa_i\lambda_i}]^2 \tag{26}$$

When the reorganization energies λ_i are close to each other, the nonparabolicity parameter κ in eq 24 tends to infinity and one obtains the standard Marcus−Hush parabolas by expanding eq 26 in $1/\kappa$. From eq 26, the activation energy of ET is

$$\Delta F_i = F_i(0) - F_{0i} = \kappa_i[\sqrt{X_{0i} + \kappa_i\lambda_i} - \sqrt{\kappa_i\lambda_i}]^2 \tag{27}$$

C. Qualitative Results. The three-parameter model predicts some novel results regarding the dependence of the reaction rates on the free energy gap (energy gap law). To illustrate them, we will consider the transition from the activated normal region to the activated inverted region through the activationless transition for the forward reaction $1 \rightarrow 2$ and the backward reaction $2 \rightarrow 1$ while maintaining $\lambda_1 < \lambda_2$ and the definition of the free energy gap as $\Delta F_0 = F_{02} - F_{01}$ (Figure 2). Our analysis here assumes $\chi_{0i} \gg 1$, which holds for most cases of interest. For the forward reaction $1 \rightarrow 2$, the transition from the normal to the inverted region is marked by the equation $X_{01} = 0$, which corresponds to a line in the space of parameters $\lambda_2/\lambda_1 > 1$ and $\Delta F_0/\lambda_1$ (Figure 4)

$$\Delta F_0/\lambda_1 = \kappa(\kappa + 1) - (\kappa - 1)^2(\lambda_2/\lambda_1) \tag{28}$$

The line shrinks into the point $\Delta F_0/\lambda_1 = \pm 1$ in the Marcus−Hush limit of equal reorganization energies (marked as "MH" in Figure 4).

Lowering the free energy gap in the inverted region for the forward reaction $1 \rightarrow 2$ leads to a new region of ET absent in the Marcus−Hush theory. When the boundary of the band of allowed energy gaps X_0 crosses the transition state $X = 0$, the

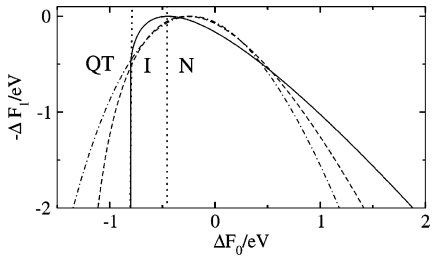

Figure 5. Energy gap law for the reaction $1 \rightarrow 2$ ($\lambda_1 < \lambda_2$) at $\lambda_1 = 0.2$ eV and $\lambda_2 = 0.25$ eV (dash−dotted line), $\lambda_2 = 0.4$ eV (dashed line), and $\lambda_2 = 2$ eV (solid line). The dotted lines separate the normal (N), inverted (I), and quantum tunneling (QT) regions for $\lambda_2 = 2$ eV.

classical crossing point of two free energy surfaces falls outside the range of allowed reaction coordinates. No crossing of free energy surfaces $F_i(X)$ is then possible ($\Delta F_0 = -7$ eV in Figure 3a), and the classical reaction channel is closed, $\Delta F_1 = \infty$. The reaction occurs only through vibrational excitations of the final ET state 2 effectively lowering the free energy gap. The transition to this new region, which may be called the "quantum tunneling region" ($\Delta F_1 = \infty$ in Figure 4a), is marked by the line $X_0 = 0$ in the space of parameters λ_2/λ_1 and $\Delta F_0/\lambda_1$.

Due to the asymmetry of the free energy surfaces for $\lambda_2/\lambda_1 > 1$, the normal region spans different ranges of ΔF_0 for positive and negative free energy gaps. Figure 4 shows a broader normal-range ET for $\Delta F_0 > 0$. This observation suggests that the goal of bringing the exothermic recombination reaction to the normal region (Figure 1) is easier to achieve when the reorganization energy of the charge-separated state D^+-A^- is much higher than the reorganization energy of the ground-state D−A (see Discussion).

The overall classical energy gap law (no vibrational excitations) for the present model is illustrated in Figure 5. With increasing the ratio of the reorganization energies λ_2/λ_1, the bell-shaped dependence of $-\Delta F_1$ on ΔF_0 becomes increasingly shallow in its right wing with positive energy gaps $\Delta F_0 > 0$, approaching the linear energy gap law $\Delta F_1 \propto \Delta F_0$. On the other hand, the approach of the fluctuation boundary X_0 to the transition point $X = 0$ squeezes the left wing narrowing the inverted region of ET.

The quantum vibronic excitations of the donor−acceptor complex can be included in the standard way by considering the Franck−Condon weighted density of states (FCWD) as a Poisson-weighted sum over the vibronic excitations leading to n vibrational quanta in the final ET state.[4] For instance, for the forward reaction one gets

$$\mathrm{FCWD}(X;1\rightarrow 2) = \mathrm{e}^{-S}\sum_{n=0}^{\infty}\frac{S^n}{n!}\mathrm{e}^{-\beta F_{1n}(X)} \qquad (29)$$

Here, $S = \lambda_i/\hbar\omega_v$ is the Huang−Rhys factor, ω_v is the characteristic vibrational frequency, and $F_{1n}(X)$ is obtained from eq 9 by replacing there X_0 with

$$X_{0n} = X_0 + n\hbar\omega_v \qquad (30)$$

The Arrhenius factor for the rate constant can be obtained (within a factor) by putting $X = 0$ in eq 29. Since the thermodynamic stability of the nuclear fluctuations requires $X < X_{0n}$, only terms corresponding to $X_{0n} > 0$ in eq 30 will contribute to FCWD(0,1→2). This fact implies a modification of the standard picture of the FCWD made of a Poisson-weighted sum of vibronic transitions. Vibronic transitions with $n < -X_0/(\hbar\omega_v)$ will not contribute to the FCWD as is illustrated by $n = 0$ and $n = 3$ in Figure 6. Only starting from the vibrational excitation number making X_{0n} positive ($n = 6$ in Figure 6) will a given vibronic transition contribute to the FCWD. This fact will result in a greater asymmetry of emission lines making the red-side wing of an optical band more shallow than the blue-side wing.

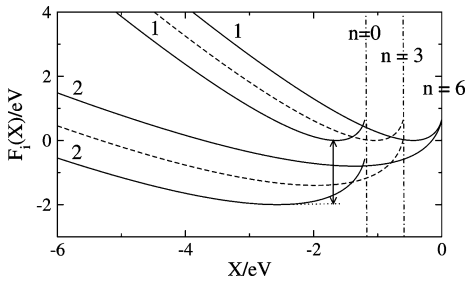

Figure 6. Inverted-region reaction $1 \rightarrow 2$ with $\lambda_1 = 0.2$ eV, $\lambda_2 = 1.0$ eV, and $\Delta F_0 = -2$ eV (shown by the vertical arrow). Classical transitions between vibrationally ground-state surfaces are forbidden by the condition $X_0 < 0$. The dashed surfaces obtained for $n = 3$ do not contribute to the Franck−Condon weighted density of states since $X_0 + n\hbar\omega_v < 0$ for $n = 3$. For $n \geq 6$, $X_0 + n\hbar\omega_v > 0$ ($\hbar\omega_v = 0.2$ eV), and these vibronic transitions contribute to the overall density of states. The dash−dotted lines indicate the fluctuation boundary X_{0n} at $n = 0$ and $n = 3$; $X_{0n} = 0$ at $n = 6$.

III. Electron Transfer in Ferroelectrics

Equation 14 for the solvent reorganization energies of a polarizable donor−acceptor complex is the central result of the formal theory relevant to our discussion of reorganization anisotropy in ferroelectrics. Equation 14 predicts that the polarizability change $\Delta\alpha$ couples to the macroscopic and local (reaction) fields to modify the change in the solute dipole moment in the course of electronic transition. Depending on the relative signs of Δm and $\Delta\alpha(R_i + F_m)$, the solute polarizability may increase or decrease the solvent reorganization energy compared to the nonpolarizable limit. The main question in this regard is whether the term $\Delta\alpha(R_i + F_m)$ can achieve a magnitude comparable to Δm. Below, we address this question by MC simulations of a model donor−acceptor diatomic in a dipolar ferroelectric solvent. Here, we first provide some relevant estimates.

The mean-field Weiss theory of spontaneous dipolar polarization[21] relates the macroscopic field in a sample of aligned dipoles m to their number density ρ as

$$F = (4\pi/3)\rho m \qquad (31)$$

The term $\Delta\alpha F_m/m$ at $\rho^* = \rho\sigma^3 = 0.7$ is then $\simeq 3\Delta\alpha/\sigma^3$ when the solute dipole is aligned with the macroscopic field; σ is the solvent diameter. The polarizability change may vary substantially between different donor−acceptor units, but the ground-state polarizability is close to $\sigma_0^3/16$ for many molecular systems (σ_0 is the effective solute diameter). If $\Delta\alpha$ is of the same order of magnitude as the ground-state polarizability, $3\Delta\alpha/\sigma^3$ scales as $(\sigma_0/\sigma)^3$. For example, for primary charge separation in *Rhodobacter sphaeroids*, $\Delta m \simeq 53$ D.[24] If we accept $\sigma = 2.87$ Å and $m = 1.83$ D for water and $\Delta\alpha \simeq 800$ Å,[15] then $\Delta m/m \simeq 29$ and $\Delta\alpha F_m/m \simeq 100$, thus resulting in comparable order-of-magnitude contributions from the change in the permanent charges and from the interaction of the polarizability change with the nonhomogeneous electric field. In addition, from the estimate of the local electric field of the protein matrix at the position of the primary pair[14] $F \simeq 10^7$ V/cm, the induced dipole $\Delta\alpha F \simeq 27$ D is also comparable to $\Delta m \simeq 53$ D.

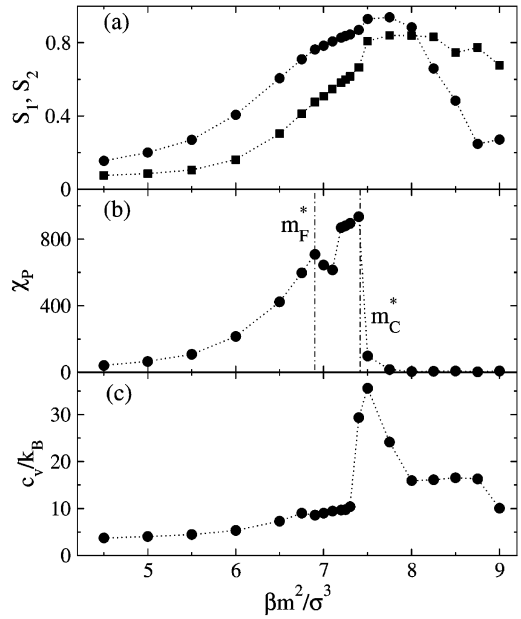

Figure 7. First (S_1, circles) and second (S_2, squares) order parameters of the fluid of dipolar soft spheres vs $\beta m^2/\sigma^3$ (a). Also shown are the dipolar susceptibility χ_P (b) and constant-volume heat capacity c_V (c). The dotted lines connect the simulation points. The dash−dotted lines in (b) indicate the points of phase transition to ferroelectric fluid (m_F*) and fcc crystal (m_C*).

A. Simulations. A fluid of soft spheres is known to spontaneously form a ferroelectric liquid phase when conducting boundary conditions are employed in the simulation protocol.[20] This system was used here to model a disordered phase with a molecular-scale macroscopic polarization coupled to the electronic states of the donor−acceptor complex. Two sets of simulations have been carried out. The fluid of soft dipolar spheres was simulated in the first set in order to establish the range of parameters for which the ferroelectric phase can be detected. This was followed by the second set of simulations in which polarizable donor−acceptor complex was dissolved in the ferroelectric liquid.

MC simulations of the pure solvent employed NVT ensemble of $N = 500$ particles in a cubic simulation cell at the reduced density of $\rho^* = \rho\sigma^3 = 0.7$. The molecules are interacting with the potential

$$v(12) = 4\epsilon(\sigma/r_{12})^{12} - \mathbf{m}_1 \cdot \mathbf{T}_{12} \cdot \mathbf{m}_2 \qquad (32)$$

where ϵ is the repulsion energy, σ is the diameter, $\mathbf{m}_j$ is the dipole moment with the magnitude m, $\mathbf{T}_{12} = \nabla_1\nabla_2 r_{12}^{-1}$ is the dipolar tensor, and $r_{12} = |\mathbf{r}_1 - \mathbf{r}_2|$. Simulations were done at $\beta\epsilon = 1.35$ and varying reduced dipole $(m^*)^2 = \beta m^2/\sigma^3$. Periodic boundary conditions and reaction-field correction for dipolar interactions with conducting boundary conditions[25] have been employed. The length of simulations was 10^6 cycles long, far from the transition point, and up to 10^7 cycles long close to the transition to ferroelectric phase.

Transition to ferroelectric phase was monitored by calculating the first-order, S_1, and second-order, S_2, parameters (Figure 7a). The first-order (ferroelectric) parameter quantifies the spontaneous polarization

$$S_1 = M/Nm \qquad (33)$$

where $\mathbf{M}$ is the total dipole moment of the solvent. The second-order (nematic) parameter is defined as the largest eigenvalue of the ordering matrix[25]

$$\mathbf{Q} = (2N)^{-1} \sum_j (3\hat{\mathbf{e}}_j\hat{\mathbf{e}}_j - \mathbf{1}) \qquad (34)$$

where $\hat{\mathbf{e}}_j = \mathbf{m}_j/m$.

Both order parameters change smoothly with m* and do not allow a reliable identification of the transition point.[26] Susceptibilities, which are expected to show sharp spikes at the points of phase transition,[27] are better indicators. Indeed, the dielectric susceptibility

$$\chi_P = (\beta/V)\langle(\delta\mathbf{M})^2\rangle \qquad (35)$$

shows the first peak at $(m_F^*)^2 = 6.9$ and the second peak at $(m_C^*)^2 = 7.5$ (Figure 7b), where V in eq 35 is the solvent volume. The heat capacity

$$c_V = 3/2 + \beta^2\langle(\delta E)^2\rangle/N \qquad (36)$$

on the contrary, shows only a little bump at m_F* and a strong peak at m_C* (Figure 7c), where E in eq 36 is the total energy of the fluid. The order parameters also show weak discontinuities at m_C*. The examination of the density structure factors reveals that the system is in the liquid state below m_C* and crystallizes into an face-centered cubic (fcc) lattice at this value of the reduced dipole. The point m_F* corresponds to the transition to a ferroelectric liquid. Note that the value of m_F* obtained here is very close to that predicted by a linear extrapolation of the phase transition line recently reported by Weis[26] for dipolar hard spheres.

The ferroelectric liquid at $(m^*)^2 = 7.0$, $\rho^* = 0.7$, and $\beta\epsilon = 1.35$ was used to study the dependence of the solvent reorganization energy on solute polarizability. In these simulations, a donor−acceptor diatomic made of two hard fused spheres of diameters $\sigma_0/\sigma = 1.5$ with the center-to-center separation $d/\sigma = 0.6$ was inserted in the center of a cubic simulation cell containing $N = 500$ soft dipolar particles at $\rho^* = 0.7$. Two opposite charges $q_0^* = \beta|q_0|/\sigma = 10$ where placed at the centers of two spheres in the charge-separated state thus producing the dipole moment $m_{02} = d|q_0|$. The induced point dipole moment $\mathbf{p}_{0i} = \hat{\mathbf{e}}_0\alpha_{0i}R_i$, caused by the dipolar polarizability α_{0i} and reaction field R_i, is placed at the midpoint of the line connecting the two centers of the diatomic. $\mathbf{p}_{0i}$ is aligned along the unit vector $\hat{\mathbf{e}}_0$ along the same line. The solute-induced dipole was equilibrated at each instantaneous configuration of the solvent by iteration algorithm (more details on the simulation protocol are given in ref 19). Ewald sums with conducting boundary conditions[25] were used to calculate the solute−solvent electrostatic interactions.

Some complications arise from the fact that the director, $\hat{\mathbf{d}} = \mathbf{M}/Nm$, fluctuates in the simulations. In real liquid crystals, fluctuations of the macroscopic director occur on the time scale of microseconds to seconds,[28] much slower than orientational motions of molecular solutes. The director, therefore, does not fluctuate on the time scale of the reaction. To account for this hierarchy of relaxation times, the simulation protocol was set up to keep the orientation of the donor−acceptor complex fixed relative to the director. The initial configuration was created by inserting a sphere of diameter σ_0 into the soft dipolar solvent followed by a short, 5×10^3 cycles, equilibration run designed to establish the director $\hat{\mathbf{d}}$. The two spheres making the diatomic were then pulled apart at a given angle to the director, and this angle was adjusted after each cycle over the N solvent molecules. The data were collected from simulation runs of 6×10^5 to 1.2×10^6 cycles. In the present simulations, the long axis of the diatomic was always aligned with the director in

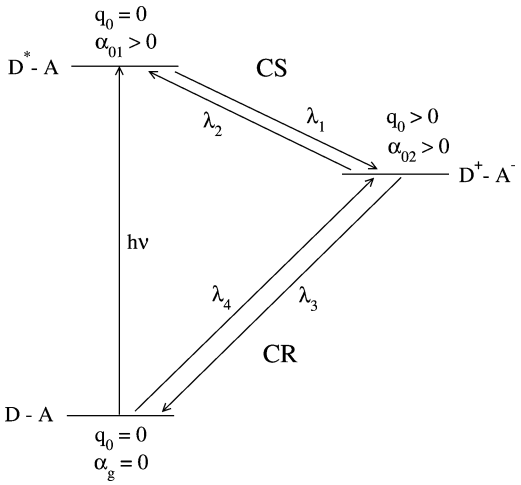

Figure 8. Charges and polarizabilities of the donor−acceptor complex in three states involved in photoinduced charge separation (CR) and charge recombination (CR).

TABLE 1: Energetic Parameters (eV) of the Charge Separation Reaction (Figure 8) in Which α_{01} Is Varied and $\alpha_{02}/\sigma^3 = 0.2$ Is Kept Constant; $\beta q_0/\sigma = 10$ in the Charge-Separated State

α_{01}/σ^3	λ_1[a]	λ_2	ΔX_0[b]	ΔX_0[c]
0.2	0.324	0.456	0.817	0.770
0.3	0.344	0.371	0.750	0.715
0.4	0.373	0.295	0.706	0.665
0.5	0.477	0.229	0.704	0.666
0.6	0.587	0.171	0.665	0.647
0.7	0.761	0.123	0.612	0.640
0.8	1.314	0.083	0.645	0.733

[a] Calculated from the simulation data assuming $\beta = 40$ eV^{-1}. [b] From the simulation data. [c] From eq 38.

such a way that the charge-transfer dipole $\Delta\mathbf{m}_0$ is always parallel to the macroscopic field **F**.

B. Energetics of Photoinduced Electron Transfer. We have followed the basic design of photoinduced ET outlined in Figure 1 and detailed in terms of charges and polarizabilities in Figure 8. It is assumed that the donor−acceptor complex has no appreciable dipole moment and polarizability in its ground state ($q_0 = 0$, $\alpha_g = 0$). Photoexcitation of the donor to state D*−A lifts the polarizability to $\alpha_{01} > 0$ but does not substantially change the charge distribution, $q_0 = 0$. Both the charge distribution and polarizability change upon charge separation resulting in D^+-A^- state ($q_0 > 0$, $\alpha_{02} > 0$). Because of the coupling of the polarizability to the reaction field R_i and the macroscopic electric field F_m (eq 14), the reorganization energies will differ for forward and backward electronic transitions for both the charge separation and charge recombination steps of the reaction mechanism. Therefore, we need four reorganization energies, λ_1 and λ_2 for charge separation and λ_3 and λ_4 for charge recombination (Figure 8).

The reorganization energies were calculated from MC configurations as second cumulants of the solute−solvent interaction potential.[19] The polarizability of the photoexcited state α_{01} was varied at constant $\alpha_{02}/\sigma^3 = 0.2$ for charge separation and the polarizability of the charge-transfer state α_{02} was varied at $\alpha_g = 0$ for charge recombination. Tables 1 and 2 and Figure 10 summarize the forward and backward reorganization energies for charge-separation and charge-recombination reactions along with the Stokes shift

$$\Delta X_0 = X_{01} - X_{02} \tag{37}$$

TABLE 2: Energetic Parameters (eV) of the Charge Recombination Reaction (Figure 8) for Which α_{02} Is Varied and $\alpha_g = 0$ Is Kept Constant; $\beta q_0/\sigma = 10$ in the Charge-Separated State

α_{02}/σ^3	λ_3[a]	λ_4	ΔX_0[b]	ΔX_0[c]
0.0	0.369	0.279	0.649	0.642
0.2	0.654	0.284	0.911	0.871
0.3	1.115	0.287	1.115	1.051
0.4	1.466	0.290	1.466	1.352
0.5	2.270	0.293	2.270	1.728
0.6	2.562	0.296	2.562	2.357
0.7	3.240	0.299	3.240	2.928
0.8	7.466	0.303	4.079	3.446

[a] Calculated from the simulation data assuming $\beta = 40$ eV^{-1}. [b] From the simulation data. [c] From eq 38.

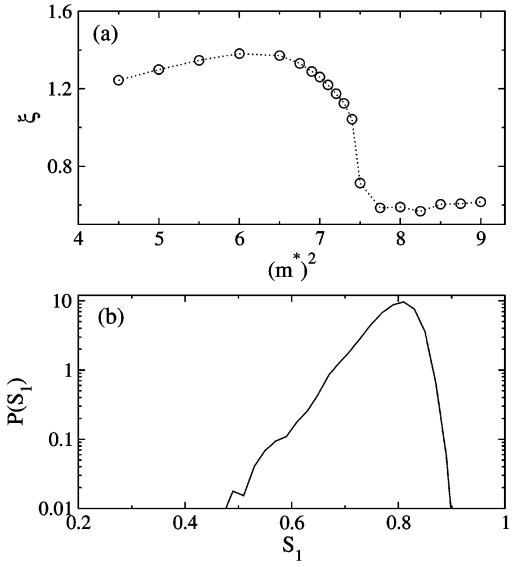

Figure 9. The linear response parameter ξ from eq 40 (a) and the distribution function of the ferroelectric order parameter (b) obtained from MC simulations at $(m^*)^2 = 7.0$, $\beta\epsilon = 1.35$, and $\rho^* = 0.7$. The dotted line in (a) connects the simulation points.

From eq 20, the Stokes shift becomes

$$\Delta X_0 = \kappa(\lambda_2 - \lambda_1) - \lambda_2 \tag{38}$$

The Stokes shift in eq 37 is equivalent to the difference of absorption and emission maxima due to eq 1. Equation 38 also applies to the Stokes shift defined in terms of two first spectral moments

$$\Delta X_0 = \langle X \rangle_1 - \langle X \rangle_2 \tag{39}$$

in the limit $\kappa_i\sqrt{\beta\lambda_i} \gg 1$.

The direct comparison of the results of simulations to the three-parameter model discussed in section II is complicated by the narrow range of solvent dipoles for which ferroelectric phase can be detected. The close proximity of two-phase transition points makes the statistics of polarization fluctuations non-Gaussian, in contrast to the Gaussian approximation adopted in eq 6. There are several indications of significant deviations from the Gaussian statistics. The ratio

$$\xi = -\langle v_{ss} \rangle / \beta \langle (\delta v_{ss})^2 \rangle \tag{40}$$

is equal to 1 ($\xi = 1$) when polarization fluctuations are Gaussian (linear response approximation).[29] Here, $\langle v_{ss} \rangle$ is the average electrostatic interaction energy of a liquid particle with the rest of the $N - 1$ particles in the liquid and $\langle (\delta v_{ss})^2 \rangle$ is the variance

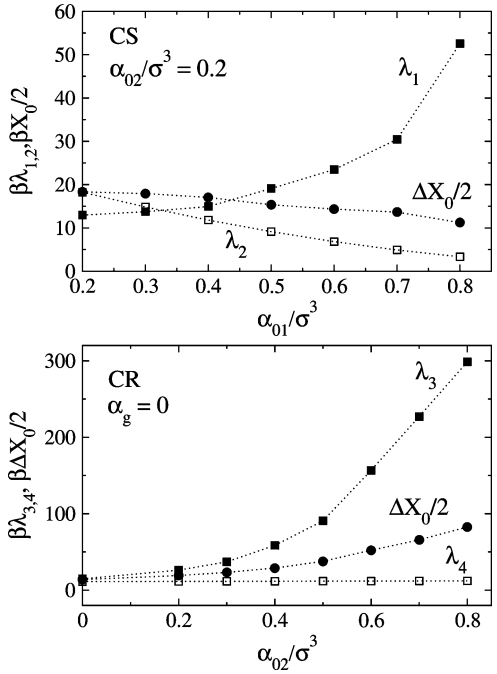

Figure 10. Reorganization energies and the Stokes shifts for the charge separation (CS) and charge recombination (CR) reactions (Figure 8) vs polarizability of the photoexcited state α_{01} (CS) and the polarizability of the charge-separated state α_{02} (CR); $q_0^* = 10$, $\alpha_g = 0$.

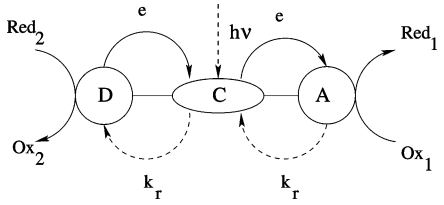

Figure 11. Reaction center model.[30,31] The unit C is photoexcited to obtain the electron from donor D and transfer it to acceptor A. The recombination rates k_r at each stage should be sufficiently low to allow normally slow catalytic reduction ($Ox_1 \rightarrow Red_1$) and oxidation ($Red_2 \rightarrow Ox_2$) reactions to occur.

of this electrostatic interaction. As is seen from Figure 9a, this parameter is higher than 1 in the paraelectric phase and drops sharply at the transition to the ferroelectric phase. In addition, the distribution of macroscopic polarization M in the simulation box is non-Gaussian. A shoulder seen in Figure 9b points to the importance of a $\propto M^4$ term in the polarization functional such as that present in the Landau theory of phase transitions.[28]

In terms of solvation properties, in the absence of polarizability change of the solute, $\Delta X_0/2$ should be equal to $\lambda = \lambda_1 = \lambda_2$. The first lines in Tables 1 and 2 correspond to exactly this situation. The difference between two reorganization energies, as well as deviations of both of them from $\Delta X_0/2$, is another indication of the non-Gaussian statistics of the solvent polarization leading to nonlinear solvation. Despite these complications, the direct calculations of the Stokes shift from simulations compare semiquantitatively to the results of applying eq 38 (Tables 1 and 2). The analytical model developed in section IIB, therefore, captures the basic thermodynamics of ET with markedly different reorganization energies.

IV. Discussion

The basic design of an artificial photosynthetic device, as advanced by Meyer and co-workers,[30,31] is shown in Figure 11. It anticipates the creation of ordered arrays where donors and acceptors are connected to catalytic sites where high-energy reactions can occur (e.g., splitting of water or reduction of carbon dioxide to carbohydrates). This design requires efficient separation of the electron and the hole. Unless this separation is achieved by high mobility of each charge in molecular arrays[32] or in valence and conduction bands of a semiconductor,[33] a high branching ratio between charge separation and charge recombination is required at each step of productive charge transfer to facilitate the redox reactions which are normally significantly slower than ET steps.

The model presented here offers some novel opportunities in terms of varying the parameters of ET reactions and activation barriers. The model emphasizes the coupling of the solute polarizability change, achieved in the course of electronic transition, to the electric field at the position of the donor−acceptor complex. The electric field has two components, the reaction field of the polar environment R_i and the macroscopic field F_m. The coupling of the overall field $R_i + F_m$ to the polarizability change creates the effective dipole moment change of the donor−acceptor complex (eq 14)

$$\Delta m_{\mathrm{eff},i} = \Delta m + \Delta\alpha(R_i + F_m) \tag{41}$$

The reaction field R_i, which depends on the electronic state of the donor−acceptor complex, is responsible for the distinction between the forward and backward reorganization energies, $\lambda_1 \neq \lambda_2$ and $\lambda_3 \neq \lambda_4$ as is shown in Figure 10 and listed in Tables 1 and 2. Note that the asymmetry in the reorganization energies up to a factor of 25 obtained in our simulations (Table 2) is the largest ever observed in either computer or laboratory experiment.

A note on the dual nature of the reorganization energy is relevant here. The reorganization energy for each ET state is calculated on the configurations of the solvent in equilibrium with the donor−acceptor complex in that given state. Therefore, the reorganization energy carries information about a particular electronic state of the donor−acceptor complex. On the other hand, the value that is being averaged is the change in the interaction potential, which is a characteristic of a given transition. As a result of this duality, the electronic charge separated state of the donor−acceptor complex D^+-A^- can be characterized by two, generally unequal, reorganization energies λ_2 and λ_3 reflecting transitions to two different electronic states, photoexcited and ground.

In the present picture, all reorganization energies λ_1, λ_2, λ_3, and λ_4 are allowed to be different, producing reach energetics of photoinduced charge separation and charge recombination. The difference in scenarios for photoinduced ET in the Marcus−Hush model and in the present formulation is illustrated in Figure 12. The plots show the free energy surfaces vs the reaction coordinate corresponding to the energy gap X between the charge-separated and photoexcited states. The energy gap for the charge recombination reaction is then $-\Delta F_{\mathrm{CS}} - \Delta F_{\mathrm{CR}} + X$, where $\Delta F_{\mathrm{CS,CR}}$ values are the free energy gaps for charge-separation and charge-recombination reactions. In the Marcus−Hush model, activationless charge separation and charge recombination is achieved at the photoexcitation energy $h\nu = 2\lambda$ (Figure 12a). Therefore, the desire to move the recombination reaction to the normal region requires energetic efficiency of the photosynthetic apparatus to be below 50% (dashed line in Figure 12a). This situation changes when different reorganization energies are allowed in the construction of the free energy surfaces. The plots in Figure 12b are made with $\lambda_2/\lambda_1 = 10$ and $\lambda_3/\lambda_4 = 5$. When activationless reactions are realized for $1 \rightarrow 2$ and $2 \rightarrow 3$ transitions, the asymmetry of the energy gap law

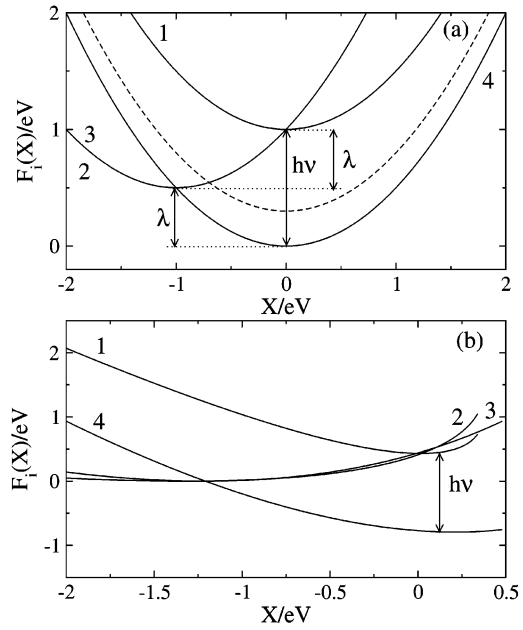

Figure 12. Free energy surfaces of photoinduced ET in the Marcus−Hush picture (a) and in the present model with different reorganization energies (b). The free energy surfaces are plotted against the reaction coordinate corresponding to the energy gap between the charge-separated and photoexcited states. The parameters are chosen to show the activationless pathway from the photoexcited state 1 to the charge-separated state 2 and from 2 to the ground state 3. The free energy surfaces 2 and 3 coincide in the Marcus−Hush picture but are distinct in the present model. In (a) the dashed line indicates the free energy surface for the normal-region charge recombination when energetic efficiency is below 50%; $h\nu$ indicates the energy of photoexcitation. The reorganization energies are $\lambda = 1$ eV (a) and $\lambda_1 = 0.2$ eV, $\lambda_2 = 2.0$ eV, $\lambda_3 = 1.0$ eV, and $\lambda_4 = 0.5$ eV (b).

leads to a higher energetic efficiency of 70%. The disadvantage of this scheme is a shallow shape of the charge-separated free energy surface making activation energy for charge recombination rather weakly dependent on changes in the free energy gap.

The role of the reaction field factor in eq 41 will diminish in weakly polar media characteristic of protein electron transfer. The effect of a strong local electric field F_m then becomes more important. If the term $\Delta\alpha R_i$ is small compared to Δm, we can simplify the effective dipole moment change to the form

$$\Delta m_{\text{eff}} = \Delta m + \Delta\alpha F_m \qquad (42)$$

Since Δm_{eff} does not depend on the electronic state, the forward and backward reorganization energies are the same ($\lambda_1 = \lambda_2$, $\lambda_3 = \lambda_4$), according to the Marcus−Hush theory. However, the factor $\Delta\alpha F_m$ can be responsible for the difference in the reorganization energies between charge separation and charge recombination reactions.

Imagine a situation in which the photoexcited state is significantly more polarizable than the ground state and the charge-separated state has about the same polarizability as the photoexcited state, $\Delta\alpha_{CS} \simeq 0$. Then, in weakly polar solvents, $\lambda_1 \simeq \lambda_2$ and both reorganization energies are small because of the low polarity of the medium. For the charge recombination reaction, $\Delta m < 0$ and $\Delta\alpha_{CR} < 0$. The permanent dipole Δm and the induced dipole $\Delta\alpha F_m$ in eq 42 add up when $F_m > 0$ and subtract when $F_m < 0$. In the former case, the charge-recombination reorganization energy $\lambda_3 \simeq \lambda_4$ is higher than the charge-separation reorganization energy $\lambda_1 \simeq \lambda_2$. Note that this picture does not contradict to the energy conservation requirement given by eq 1 since the photoexcited-state D*−A and the ground-state D−A are two different electronic states characterized by different polarizabilities.

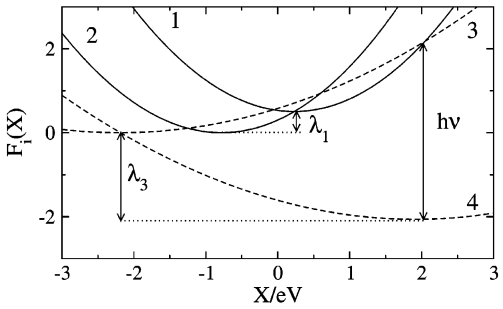

Figure 13. Free energy surfaces in the Marcus−Hush picture when the reorganization energy for charge recombination $\lambda_3 = \lambda_4 = 2.0$ eV is higher than reorganization energy for charge separation $\lambda_1 = \lambda_2 = 0.5$ eV due to the coupling of the polarizability change to the macroscopic electric field (eqs 14 and 42).

The normal-region ET can be realized within the Marcus−Hush picture when the reorganization energy is greater than the charge-recombination free energy gap $\lambda_3 > \Delta F_{CR}$ (Figure 13). As in Figure 12a, the energetic efficiency is about 50%, and it drops when charge recombination is shifted into the normal region. However, even in this limit of reduced flexibility of altering the ET parameters, the presence of the macroscopic electric field in the expression for the reorganization energy (eqs 14 and 42) opens the door to manipulations of reorganization parameters through proper design of mutual signs of the polarizability change and the direction of the macroscopic field.

We can conclude that the combination of a highly polarizable donor−acceptor complex with macroscopic electric field creates a principal possibility for suppressing the recombination reaction in photosynthetic ET. From a more general perspective, the notion of nonequal reorganization energies and nonparabolic free energy surfaces, compliant with the condition of energy conservation (eq 1), opens the door to new models of ET activation which may eventually lead to a practical solution of the photosynthesis problem.

Acknowledgment. This research was supported by the National Science Foundation (CHE-0304694).

References and Notes

(1) Marcus, R. A. *Rev. Mod. Phys.* **1993**, *65*, 599.
(2) Wasielewski, M. R. *Chem. Rev.* **1992**, *92*, 435.
(3) Gust, D.; Moore, T. A.; Moore, A. L. *Acc. Chem. Res.* **1993**, *26*, 198.
(4) Bixon, M.; Jortner, J. *Adv. Chem. Phys.* **1999**, *106*, 35.
(5) Kakitani, T.; Mataga, N. *J. Phys. Chem.* **1985**, *89*, 8.
(6) Hwang, J.-K.; Warshel, A. *J. Am. Chem. Soc.* **1987**, *109*, 715.
(7) Kuharski, R. A.; Bader, J. S.; Chandler, D.; Sprik, M.; Klein, M. L.; Impey, R. W. *J. Chem. Phys.* **1988**, *89*, 3248.
(8) Marchi, M.; Gehlen, J. N.; Chandler, D.; Newton, M. *J. Am. Chem. Soc.* **1993**, *115*, 4178.
(9) Yelle, R. B.; Ichiye, T. *J. Phys. Chem. B* **1997**, *101*, 4127.
(10) Hartnig, C.; Koper, M. T. M. *J. Chem. Phys.* **2001**, *115*, 8540.
(11) Matyushov, D. V. *J. Chem. Phys.* **2004**, *120*, 7532.
(12) Tachiya, M. *Chem. Phys. Lett.* **1989**, *159*, 505.
(13) Matyushov, D. V.; Voth, G. A. *J. Chem. Phys.* **2000**, *113*, 5413.
(14) Steffen, M. A.; Lao, K.; Boxer, S. G. *Science* **1994**, *264*, 810.
(15) Middendorf, T. R.; Mazzola, L. T.; Lao, K.; Steffen, M. A.; Boxer, S. G. *Biochim. Biophys. Acta* **1993**, *1143*, 223.
(16) Kjellberg, P.; He, Z.; Pullerits, T. *J. Phys. Chem. B* **2003**, *107*, 13737.
(17) Matyushov, D. V.; Voth, G. A. *J. Phys. Chem. A* **1999**, *103*, 10981.
(18) Small, D. W.; Matyushov, D. V.; Voth, G. A. *J. Am. Chem. Soc.* **2003**, *125*, 7470.
(19) Gupta, S.; Matyushov, D. V. *J. Phys. Chem. A* **2004**, *108*, 2087.
(20) Wei, D.; Patey, G. N. *Phys. Rev. Lett.* **1992**, *68*, 2043.
(21) Zhang, H.; Widom, M. *Phys. Rev. B* **1995**, *51*, 8951.

(22) Morozov, K. I. *J. Chem. Phys.* **2003**, *119*, 13024.
(23) Wei, D.; Patey, G. N.; Perera, A. *Phys. Rev. E* **1993**, *47*, 506.
(24) Bixon, M.; Jortner, J.; Mechel-Beyerle, M. E. *Chem. Phys.* **1995**, *197*, 389.
(25) Allen, M. P.; Tildesley, D. J. *Computer Simulation of Liquids*; Clarendon Press: Oxford, 1996.
(26) Weis, J.-J. *J. Chem. Phys.* **2005**, *123*, 044503.
(27) Binder, K.; Heermann, D. W. *Monte Carlo Simulation in Statistical Physics*; Springer-Verlag: Berlin, 1992.
(28) Vertogen, G.; Jeu, V. W. H. D. *Thermotropic Liquid Cristals, Fundamentals*; Springer-Verlag: Berlin, 1988.
(29) Matyushov, D. V.; Ladanyi, B. M. *J. Chem. Phys.* **1999**, *110*, 994.
(30) Huynh, H. V.; Dattelbaum, D. M.; Meyer, T. J. *Coord. Chem. Rev.* **2004**, *249*, 457.
(31) Alstrum-Acevedo, J. H.; Brennman, M. K.; Meyer, T. J. *Inorg. Chem.* **2005**, *44*, 6802.
(32) Hoertz, P. G.; Mallouk, T. E. *Inorg. Chem.* **2005**, *44*, 6828.
(33) Lewis, N. S. *Inorg. Chem.* **2005**, *44*, 6900.